Positive influence of femtosecond pulsed laser machining on levitation forces of top-seeded melt-grown textured YBCO

Superconductor Science and Technology

OPEN ACCESS

RECEIVED
7 February 2026

REVISED
15 March 2026

ACCEPTED FOR PUBLICATION
1 April 2026

PUBLISHED
15 April 2026

PAPER

Positive influence of femtosecond pulsed laser machining on levitation forces of top-seeded melt-grown textured YBCO

F Al-Mokdad[1], S B Guner[2,3,5], J Rivera-Sahún[4], A Badía-Majós[4], L A Angurel[4], G F de la Fuente[4], E Martínez[4], L Porta-Velilla[4] and A Gencer[3,5,*]

[1] Ankara University, Graduate School of Natural and Applied Sciences, Ankara, Türkiye
[2] Department of Physics, Faculty of Arts and Sciences, Recep Tayyip Erdogan University, 53100 Rize, Türkiye
[3] Center of Excellence for Superconductivity Research, Ankara University 06500, Golbasi, Ankara, Türkiye
[4] Instituto de Nanociencia y Materiales de Aragón (INMA), CSIC-University of Zaragoza, c/ María de Luna 3, 50018 Zaragoza, Spain
[5] Science Faculty, Physics Department, Ankara University, Ankara, Türkiye
[*] Author to whom any correspondence should be addressed.

E-mail: Ali.Gencer@science.ankara.edu.tr

Keywords: ultrashort-pulsed laser, machining, textured YBCO superconductors

Abstract

High-temperature textured YBCO superconductors are considered relevant for applications requiring strong flux pinning, and hence enhanced critical current density and resilient levitation forces, such as maglev systems, magnetic resonance imaging and nuclear magnetic resonance magnets. Improving the performance of YBCO for such applications is commonly achieved by enhancing the flux pinning properties through various mechanisms. In addition, either related to the sample fabrication process or demanded by the final operation conditions, machining these highly brittle samples would be desirable for a number of applications and is a challenging demand. This work reports on the use of ultrashort-pulsed laser irradiation to machine holes into top-seeded melt-growth YBCO samples and how this processing affects their microstructure and superconducting behavior. The x-ray diffraction (XRD) and scanning electron microscopy results demonstrate that ultrashort-pulsed laser machining can create well-defined holes with diminishing microstructural damage. The superconducting properties of the laser-machined samples are essentially preserved, even compatible with the enhancement in the critical current density and levitation force properties. These findings demonstrate the potential of ultrashort-pulsed lasers as a viable tool for machining textured YBCO products and enhancing their performance without degrading their functional properties. This method paves the way towards the generation of artificial defects, machining and shaping of high T_c superconductor ceramics into precisely well-defined complex geometries relevant for power applications.

1. Introduction

Despite the fact that nearly 40 years have passed since the discovery of high-temperature superconductors, research in this field has remained active and dedicated to optimizing their properties to meet the demands of their potential applications such as energy storage systems, magnetic bearings for motors and flywheels, magnetic resonance imaging, nuclear magnetic resonance magnets for research, and maglev transportation systems [1–7]. Among high-temperature superconductors, $YBa_2Cu_3O_{7-x}$ (YBCO and the general REBCO family superconductor, where RE stands for rare-earth elements such as Y, Gd, Sm, Nd, etc) is considered one of the most attractive superconductors for practical applications due to its chemical stability, high irreversibility line, high critical temperature of approximately 93 K [8, 9], remarkable critical current density J_c values at liquid nitrogen temperature (77 K) and superior levitation forces [10, 11]. These properties are affected by the microstructure of the samples which in turn depends

on the material's preparation processes, quality and geometry. Thus, ongoing research to better understand and optimize the properties of YBCO superconductors, their growth processes and geometries will improve their potential relevance in practical applications.

The maximum levitation forces and J_c values of YBCO superconductors are considered very important parameters for applications. These parameters can be enhanced by immobilizing the flux lines that penetrate into the material in the presence of a magnetic field. The crystalline defects and impurities in the material can work as pinning centers that prevents the motion of these flux lines. Thus, introducing artificial pinning centers (APCs) through embedding artificial defects in the crystal structure of the superconductor materials to lead the number of the flux lines pinned, plays a key role in increasing the in-field J_c and therefore enhancing the performance of superconductor at higher magnetic fields [12–14]. Several approaches and methods have been developed to generate APCs in the microstructure of YBCO superconductors, such as doping non-superconducting materials (for example: $Y_2Ba_1Cu_1O_5$ (Y211)) and other metallic oxide nanoparticles that act as three-dimensional (3D) PCs [15, 16], or by introducing one-dimensional defects by alternate methods, such as heavy-ion irradiation [17].

On the other hand, the enhancement of the levitation force of superconductors has been investigated in many studies, based on the use of different techniques [18–22]. The levitation forces are greatly dependent on the microstructure and mechanical properties of the superconductor. One of the proposed techniques is to drill artificial holes inside the YBCO samples in order to improve the chemical properties of the samples by facilitating the oxygenation process needed for the tetragonal-to-orthorhombic phase transition. As a consequence, porosity is reduced because the gases produced during melting are able to escape through the drilled holes instead of being trapped inside the samples core, as usually observed [23, 24]. Although such drilled holes are often reported to enhance oxygen diffusion and reduce cracking, a number of authors have reported contradictory results. Some studies have indicated that oxygenation is not necessarily improved by the presence of holes, and that the process may introduce additional challenges such as microcrack formation, reduce hardness, and cause local weakening of the fragile superconducting matrix [25–27]. For example, Lousberg *et al* [25] observed that mechanical drilling can alter the microstructure, leading to a greater-than-predicted decrease in trapped magnetic field, while Radušovská *et al* [28] reported that defects formed during the propagation of holes into the growing bulk can negatively affect the macroscopic superconducting properties.

Machining artificial holes into textured YBCO superconductors is considered a complex process from the technical point of view, because of the brittle character of this ceramic material, which makes it very difficult to cut or deform without inducing damage. These limitations motivate the development of alternative machining methods that can introduce artificial holes in these superconductors, aiming to improve their performance while minimizing the damage associated with conventional mechanical drilling. This method should enable 3D subtractive machining of thin and thick bulk superconductors, and should be independent of microstructure and density within the bulk superconductor. Laser machining is considered an ideal tool for precise and almost damage-free machining of YBCO superconductors because of its non-contact nature and flexibility in following any geometrical path. However, not all lasers are suitable for machining ceramics. Lasers with pulse durations exceeding tens of picoseconds (ps) or nanoseconds usually transfer significant amounts of heat to areas near the beam focus, which induces thermo-mechanical stress that leads to microcracks and an eventual catastrophic failure of the ceramic bulk body. In ceramic superconductors, this reduces J_c values because of the reduction in electrical connectivity as microstructural discontinuities develop (microcracks and other defects). In this context, ultrashort laser-matter interaction with REBCO superconductors has been investigated primarily in thin-film and coated-conductors. For example, Martirosian *et al* [29] reported an experimental and numerical study of femtosecond (fs) and ps laser irradiation of REBCO tapes, with particular emphasis on the influence of laser pulse energy, focusing conditions, and pulse accumulation on defect formation. While their work addresses thin films rather than bulk or textured YBCO, the qualitative discussion of laser parameter effects provides useful background for understanding laser-superconductor interaction.

This study aims to present, for the first time to the best of our knowledge, how ultrashort-pulsed lasers can be used to introduce artificial holes of various dimensions in the 3D-machined YBCO samples that are prepared by the top-seeded melt-growth (TSMG) method, and examines the effects of laser irradiation on their microstructure and superconducting properties with a particular emphasis on the levitation magnetic forces and J_c measurements. The results are compared with those obtained from conventional plain YBCO sample, i.e. sample fabricated by the same TSMG process but without any laser machining.

2. Experimental methods

In this study, Y123 ($YBa_2Cu_3O_{7-x}$) and Y211 powders were prepared using the conventional solid-state reaction method. High-purity precursor powders (Y_2O_3 (99.98%), $BaCO_3$ (99.98%), and CuO (99.99%)) were mixed according to the stoichiometric ratios. The mixtures were then calcined at 900 °C for 20 h and 920 °C for 15 h, respectively. Subsequently, quasi-single-crystal samples were fabricated by the TSMG method. A mixture of 75 wt% Y123 and 25 wt% Y211 powders, with an addition of 0.5 wt% CeO_2, was mixed for 1–2 h to achieve homogeneity. The addition of CeO_2 was selected based on its well-established role as a cost-effective grain refining chemical agent used to refine the size and distribution of RE-211 inclusions (Y211 phase in this study) within the final sample microstructure [3, 30, 31]. Finer size of Y211 secondary phase particles, helps in the formation of chemical flux pinning centers and enhances critical current density in melt-processed YBCO bulks [32]. The concentration of 0.5 wt% of CeO_2 was chosen because previous studies indicate that low doping level is sufficient to achieve effective Y211 refinement without introducing excessive secondary phases or degrading the superconducting matrix [33–37]. The mixture was then uniaxially pressed into pellets with a diameter of 32 mm using a hydraulic press under a load of 1.5 tons. Nd-123 ($Nd_{1.8}Ba_{2.4}Cu_{3.4}O_7$) seeds of similar dimensions (approximately 3 mm × 2 mm × 2 mm) were placed on the top surface of the pellets [33]. Nd-123 was selected as the seed material because it possesses three key characteristics essential for an effective seed crystal [3]. First, it exhibits the highest peritectic decomposition temperature among REBCO superconductors, ensuring thermal stability during melt processing. Second, its lattice parameters are closely matched to those of Y123, promoting epitaxial alignment. Third, Nd-123 demonstrates excellent phase stability in Ba–Cu–O liquid containing RE ions at elevated temperatures, which facilitates the nucleation and growth of large single-grain Y123 superconductors [38, 39].

The samples were sintered at 1040 °C for 1 h with a heating rate of 150 °C h^{-1}. The temperature was then decreased to 1005 °C at a cooling rate of 40 °C h^{-1}, followed by a further decrease to 960 °C at a rate of 0.3 °C h^{-1}. Finally, the samples were cooled to room temperature at a rate of 200 °C h^{-1}.

All samples were polished before further processing, and their thicknesses ranged between 4.5 mm and 5 mm. Five well-grown YBCO samples were obtained. Sample A is the conventional plain sample without laser machining while the other four samples (B, C, D and E) were machined with the fs green laser (CARBIDE CB3+CBM03-2H–3H fs laser system with a harmonics module incorporated). A periodic lattice of hole-like features was introduced on both surfaces of the pellet samples, with varying hole diameters and inter-hole spacing, as summarized in table 1. The laser micromachining was performed using an average output power of 9.7 W at a resonating frequency of 200 kHz, yielding an Energy per pulse of 48.5 μJ. This was modified with a pulse picker divider of 20 to provide an effective output pulse frequency of 10 kHz. A beam scanning speed of 9 mm s^{-1} was applied during the process, which was repeated 20 times. Finally, all samples were annealed in flowing oxygen at a temperature of 450 °C for 7 d. After melt growth, Y123 bulks exhibit a non-superconducting tetragonal phase requiring oxygen annealing to achieve the superconducting orthorhombic phase [40]. Due to slow oxygen diffusion in dense ceramics, prolonged annealing (∼150–200 h) is necessary for complete bulk oxygenation [33, 41–43]. This extended duration promotes optimal oxygen ordering, enhancing superconducting properties for reliable performance [3, 44, 45]. The annealing duration was therefore selected consistent with established practice. The resulting samples after laser machining are shown in table 1.

XRD measurements were done using a Rigaku MiniFlex II-desktop x-ray diffractometer using CuK_α radiation to check the phase composition of the prepared YBCO samples. The data were collected over a 2θ range of 20°–75° at a scan speed of 2° min^{-1} at room temperature. The measurements were conducted on specimens cut from the top surface of each sample. The microstructure of the holes introduced by laser machining was investigated, and the potential for any adverse effects on sample composition was assessed using a confocal microscope (PLu 2300 optical surface profiler) and a field emission scanning electron microscope (FE-SEM, Carl Zeiss MERLIN).

For the levitation measurements, the magnetic levitation force was measured in both zero-field cooled (ZFC) and field-cooled (FC) regimes at temperatures of 37 K and 77 K using a home-made magnetic levitation force measurement system. Details about measurements and properties of this system are reported in a previous study [46]. The system employs a cylindrical Nd–Fe–B permanent magnet with a diameter of 19 mm, a thickness of 10 mm, and with surface remanent magnetic induction of approximately 0.5 T. The magnetic measurements of the samples, including M–H and AC susceptibility, were carried out using a Quantum Design SQUID magnetometer operating in vibrating sample magnetometer mode at temperatures of 37 K and 77 K. The samples for these measurements were extracted from

Table 1. Summary of fs laser machining parameters for the YBCO samples.

Sample	Machining pattern	Hole diameter (μm)	Hole spacing (mm)	Surface image
A	None	—	—	
B	Hole lattice (both surfaces)	200	0.65	
C	Hole lattice (both surfaces)	200	1.95	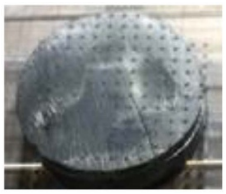
D	Hole lattice (both surfaces)	200	1.30	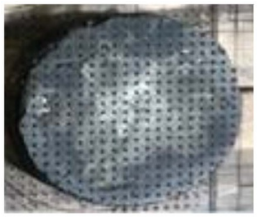
E	Hole lattice (both surfaces)	400	1.30	

Table 2. Laser-cut disc samples for magnetic measurements.

Sample name	Schematic of disc location in sample	Laser-cut disc photograph	Disc diameter (mm)	Thickness (mm)
Conventional plain sample A	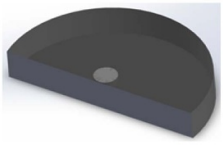		3	0.42
Laser-machined sample E	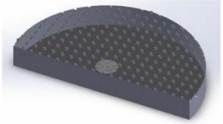		3	0.43

samples A and E by laser cutting into disc shapes with a thickness of approximately 0.4 mm and a diameter of 3 mm as shown in table 2. In all magnetization measurements, the magnetic field was applied parallel to the *c*-axis (i.e. perpendicular to the sample's surface).

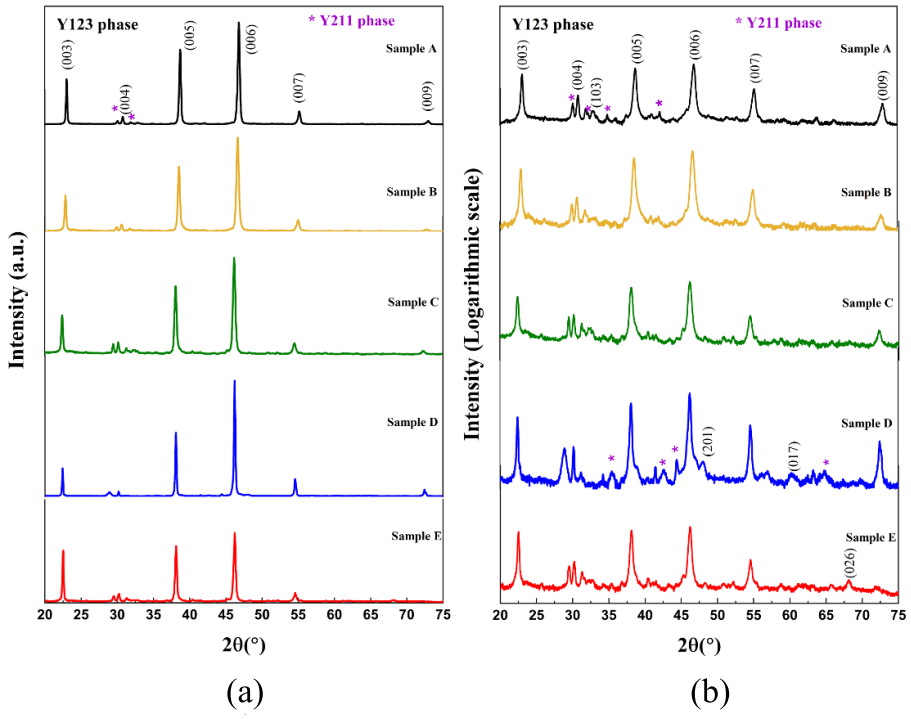

Figure 1. X-ray diffraction patterns of the samples A, B, C, D, and E with (a) linear and (b) logarithmic scale.

3. Results and discussion

3.1. Structural properties

The XRD measurements were carried out on the top surface of samples A–E at room temperature, and the obtained diffraction patterns are shown in figures 1(a) and (b) in both linear and logarithmic scale. It is observable that the major peaks in all patterns correspond predominantly to the Bragg reflections of the (00l) family, such as (003), (004), (005), (006), and (007), indicating the *c*-axis oriented crystalline nature of the Y123 phase. These results are in good agreement with the standard reference patterns reported in the ICDD Powder Diffraction File (PDF no. 01-078-2129) [47] and with previous studies on a single-domain YBCO prepared via the TSMG method [31, 33, 48]. In addition to the dominant (00*l*) reflections, minor reflections corresponding to other (*hkl*) planes of the Y123 phase are also identified, confirming the orthorhombic structure of the superconducting phase.

Minor reflections associated with the Y211 phase, marked by asterisks in figure 1, are also detected in all samples, indicating the presence of a small amount of secondary phase (PDF no. 01-078-2214) [49]. Quantitative phase analysis was performed and the obtained lattice parameters of the orthorhombic Y123 phase as well as phase percentages are summarized in table 3. The results show that the Y123 phase is highly dominant in all samples, with phase fractions exceeding 92%, while the Y211 phase is present in relatively small amounts ranging from approximately 4% to 7%. The lattice parameters *a*, *b*, and *c* of the orthorhombic Y123 phase fall within the typical ranges reported for Y123 compounds [50]. Slight variations in these parameters among the different samples may be related to minor differences in oxygen content, internal strain, or microstructural defects [51–53]. In addition, the number of holes per unit area and the total hole area may influence the related calculations. During the oxygenation process, a larger total hole area is expected to facilitate oxygen diffusion into the sample, which can consequently result in deviations from the calculated lattice parameters. Furthermore, the presence of impurities and/or minor secondary phases may contribute to the intensity of the reflections associated with specific (*hkl*) planes. The laser machining, followed by the oxygenation process, appears to be consistent with the observed increase in levitation force and the enhancement of J_c, which is discussed in more details in the results and discussion section.

The presence of the minor Y211 phase observed in the XRD patterns can be explained by the melt-growth mechanism involved in TSMG process. In general, bulk YBCO superconductors are fabricated using the melt-growth technique starting from a precursor mixture of Y123 and Y211 powders. When

Table 3. Summary of lattice parameters and phase percentages of samples A, B, C, D, and E.

	Lattice parameters			Phase percentage (%)	
Sample	*a* (Å)	*b* (Å)	*c* (Å)	Y123	Y211
A	3.818	3.881	11.628	95.87	4.13
B	3.748	3.881	11.680	94.24	5.76
C	3.780	3.784	11.785	92.60	7.40
D	3.830	3.824	11.780	94.35	5.65
E	3.809	3.788	11.775	93.06	6.94

the temperature exceeds the peritectic temperature, the Y123 phase undergoes peritectic decomposition, forming Y211 particles together with a Ba–Cu–O liquid phase [31]. Upon slow cooling through the peritectic temperature, a peritectic recombination takes place between the Y211 particles and the liquid phase, leading to the formation and growth of the Y123 superconducting matrix. However, some Y211 particles remain unreacted or partially dissolved during the growth process and therefore persist in the final material as secondary phase inclusions. These remaining Y211 particles are commonly observed in melt-grown REBCO materials and are known to contribute to enhanced flux pinning properties [31]. Nevertheless, their distribution and fraction are not easily controllable during the growth process. This behavior is reflected in the XRD results, where small diffraction peaks corresponding to the Y211 phase are detected. Therefore, presence of the characteristic Bragg reflections belonging to Y123 phase in all samples confirms that the laser machining is not harmful apart from minor but not very effective deformation on the cut surface area.

Figure 2 presents the 1D, 2D, and 3D surface profiles of the hole obtained with an optical surface profiler, respectively. As shown in the 1D surface profile, the hole has a conical rather than cylindrical geometry, which is due to the non-uniform distribution of the laser beam, typically following a Gaussian profile. Consequently, the central region is exposed to a higher energy density, resulting in greater material ablation compared to the edges. The 2D height profile displays the top-view surface morphology, indicating an almost uniform circular symmetry. Moreover, the 3D profile shows the surface topography, highlighting the smooth interior and well-defined edges of the hole.

The SEM images were scanned at both the top surfaces and the cross-sections of the samples to observe the hole geometry and internal structure. Figures 3(a)–(f) show the SEM micrographs of the samples B and E. As shown in figures 3(c) and (f), the holes exhibit a conical shape and the diameters of these holes in samples B and E (theoretically 200 μm and 400 μm) are measured to be approximately 218 μm and 361 μm, respectively, with depths of about 826 μm and 1261 μm. As discussed by Martirosian *et al* [29] in the context of ultrashort laser irradiation of REBCO thin films, where axisymmetric crater-like defects were formed under fs and *p* laser pulses, the decreasing cross section of the holes may be related to the (Gaussian) profile. In addition, a certain amount of debris is observed at the bottom of the holes, likely due to incomplete removal of ablated material, possibly caused by insufficient vacuuming during laser drilling. Finally, as shown in figures 4(a)–(f), the SEM images reveal no visible surface cracks or significant melting on the hole walls or edges of samples B and E within the applied magnification range. The observed continuity of the hole boundaries suggests the absence of macroscopic cracking induced by laser drilling.

As reported in the literature, one of the limitations associated with mechanical drilling of bulk YBCO superconductors is the formation of cracks between holes, appearing due to stress during crystal growth and/or during the oxygenation process. For example, Lousberg *et al* [25] reported cracks between mechanically drilled holes, with cracks observed on both the top and bottom surfaces of the samples. Similarly, Diko *et al* [27] showed that mechanically drilled superconducting samples developed cracks between holes, and they linked this crack formation to the stress produced during oxygenation from the surfaces of the drilled holes. In contrast, the samples processed by laser machining in the present study do not show such cracks. SEM images further confirm that the laser machining process produced clean holes without significant melting, crack formation, or visible damage in the inner surface, around and outside the holes. The latter clearly demonstrates the advantage of using a fs laser for machining YBCO superconductors.

3.2. Levitation force measurements

To investigate the potential influence of the holes introduced by laser machining and to evaluate the performance of the YBCO samples for levitation applications, magnetic levitation measurements were carried out in ZFC and FC regimes. Figure 4 summarizes all levitation force measurements, showing the

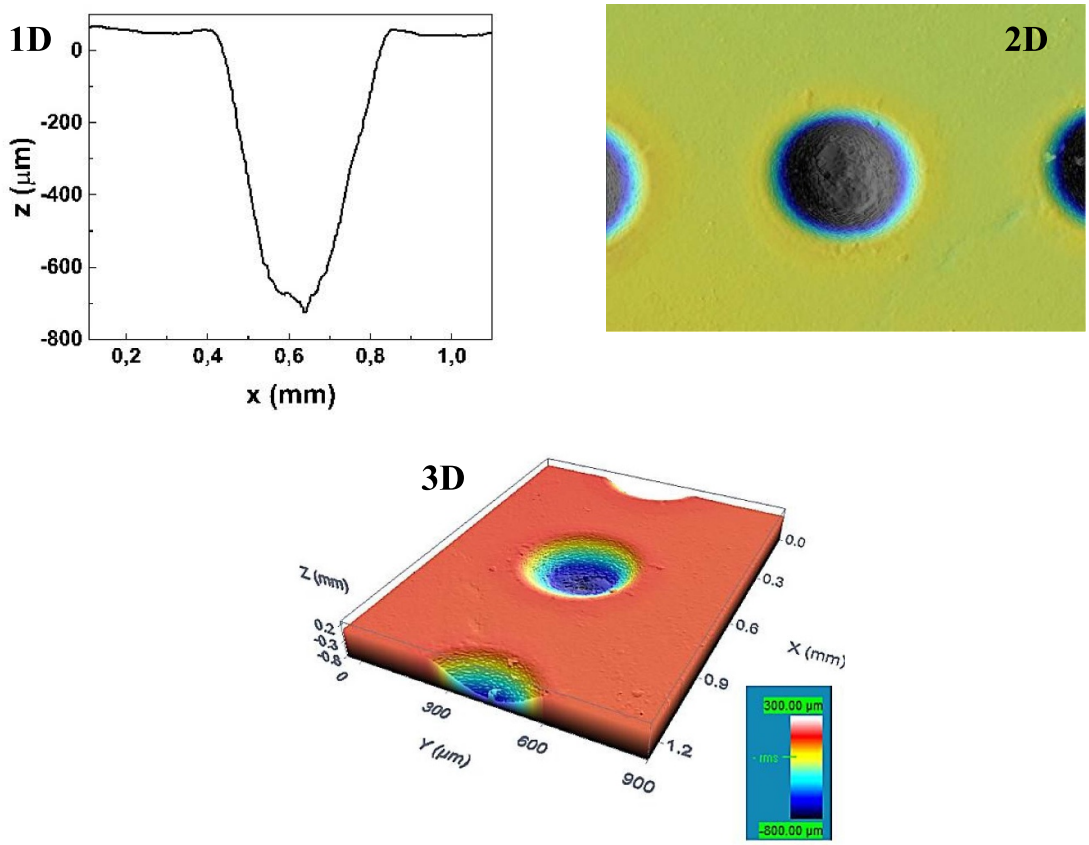

Figure 2. 1D, 2D, and 3D surface profiles of the hole measured by an optical surface profiler. The images represent the depth profile, height distribution, and three-dimensional morphology, respectively.

vertical levitation force F_z (N) as a function of the vertical displacement z (mm) between the permanent magnet and the samples in the ZFC and FC regimes at 77 K and 37 K.

As expected from the intrinsic magnetic hysteresis of the superconducting material, all the curves exhibit hysteresis loops, with a wider hysteresis loop observed at 77 K compared to 37 K. This behavior is associated with the lower critical current density at higher temperatures. At 37 K, where J_c is higher, a thin surface layer of supercurrents is sufficient to screen the magnetic flux, resulting in a nearly reversible levitation behavior. In contrast, at 77 K, the reduced J_c requires current penetration deeper into the bulk, making flux trapping effects more noticeable and leading to wider hysteresis. Moreover, it is shown that in all curves, the levitation force increases sharply as the distance between the sample and the permanent magnet decreases consistently with results reported by Güner *et al* [33] for similarly prepared YBCO samples.

In the ZFC regime (figure 4(a)), at 77 K, all laser-machined samples (B, C, D, and E) exhibit levitation forces comparable to that of the conventional plain sample (A). Among them, sample E shows the highest maximum levitation force, $F_{z\max} = 14.44$ N for the smallest distance (1.5 mm). At 37 K (figure 4(b)), all samples demonstrate slightly higher levitation forces than the plain sample, with sample E again exhibiting the highest $F_{z\max} = 20.22$ N. Notably, the laser-machined samples exhibit levitation force values that are comparable to or even exceeding that of the plain reference sample by about 13%. Accordingly, we conclude that YBCO samples do not experience any deterioration after fs laser machining, show higher performance as evident from levitation force measurements. Therefore, the results indicate that controlled hole fabrication by laser machining appears to be a promising technology in magnetic levitation applications, as it can be implemented without compromising superconducting performance.

Figures 4(c) and (d) show the vertical levitation force F_z as a function of z in the FC regime at 77 K and 37 K, respectively. In this regime, the sample is cooled close to the permanent magnet (at a distance $z = 1.5$ mm in this case), allowing magnetic flux to penetrate and become trapped inside the sample due to pinning flux, resulting in an attractive levitation force when the superconductor is moved away, as related to the induced current. All laser-machined samples show comparable and slightly higher

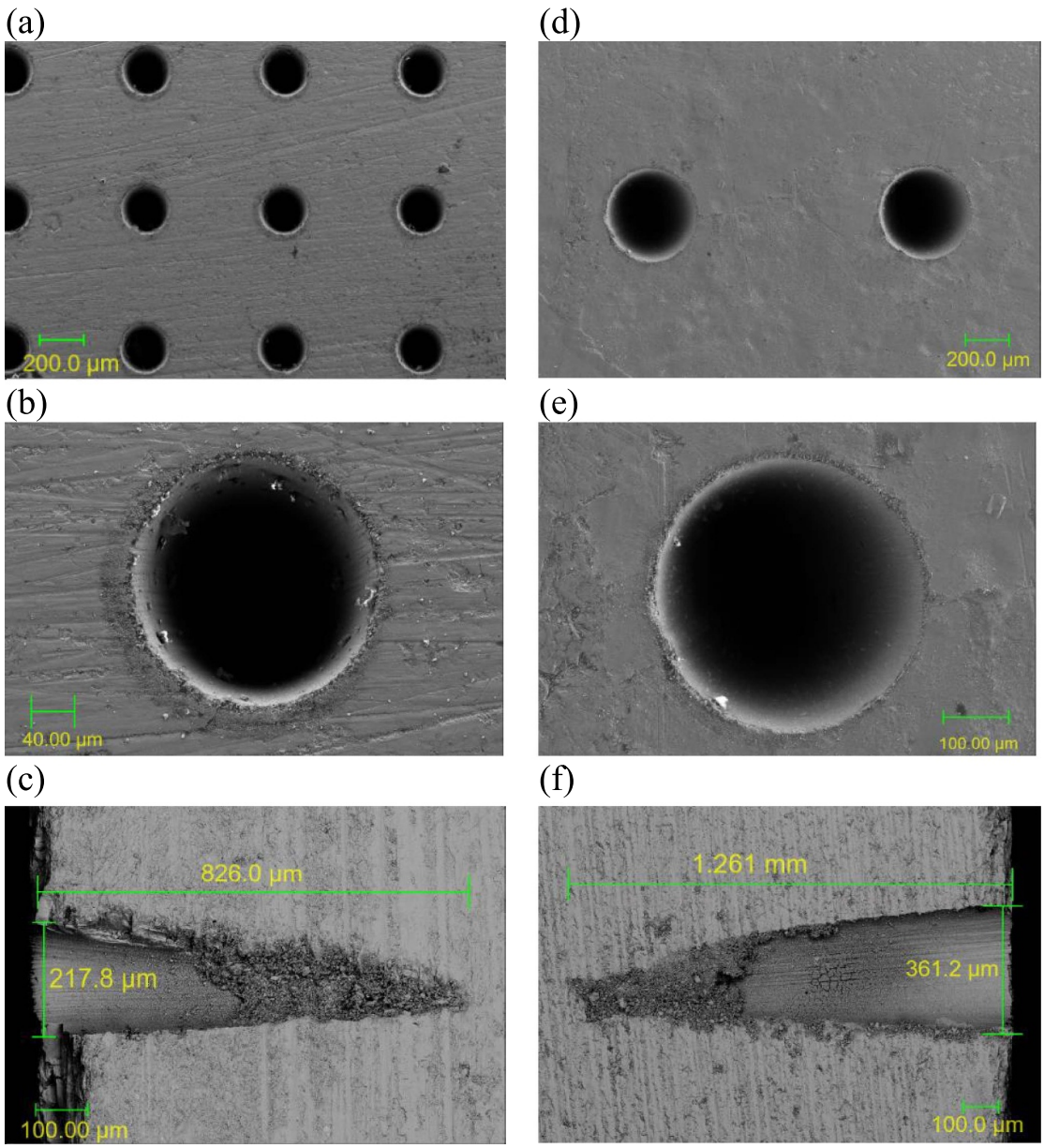

Figure 3. SEM images of laser-machined holes on samples B and E. (a)–(c) Correspond to sample B: (a), (b) top surface views at different magnifications, and (c) cross-sectional view. (d)–(f) Correspond to sample E: (d), (e) top surface views at different magnifications, and (f) cross-sectional view. Images of sample B were acquired using secondary electrons (SE2) at an accelerating voltage of 10 kV, while images of sample E were acquired using SE2 at 20 kV. Scale bars are shown on each image.

attractive forces compared with the plain sample. Overall, the ZFC regime yields stronger repulsive levitation, whereas the FC regime exhibits stronger attractive interaction and good stability, results that are consistent with literature reports [34]. The broader hysteresis loops observed at higher temperature again reflect the reduction in trapped flux and induced current strength. These results confirm that cooling conditions and sample structure both play significant roles in determining the levitation performance of YBCO superconductors.

Moreover, one of the most important factors affecting the magnetic levitation force is the critical current density. Thus, resourcing to Bean´s model [54], one may argue that the superconductor may be treated as a collection of current loops, each carrying the maximal current density. Then, the force between the magnet and the superconductor may be calculated as the summation over current loops and with the overall common factor J_c, i.e.: the net force is proportional to J_c through geometry dependent factors. The experimental results of levitation force measurements in this work show that F_z is roughly proportional to J_c confirming this thesis. As it will be later confirmed by magnetic moment measurements, the laser-machined sample (E) has slightly higher critical current density compared to the plain

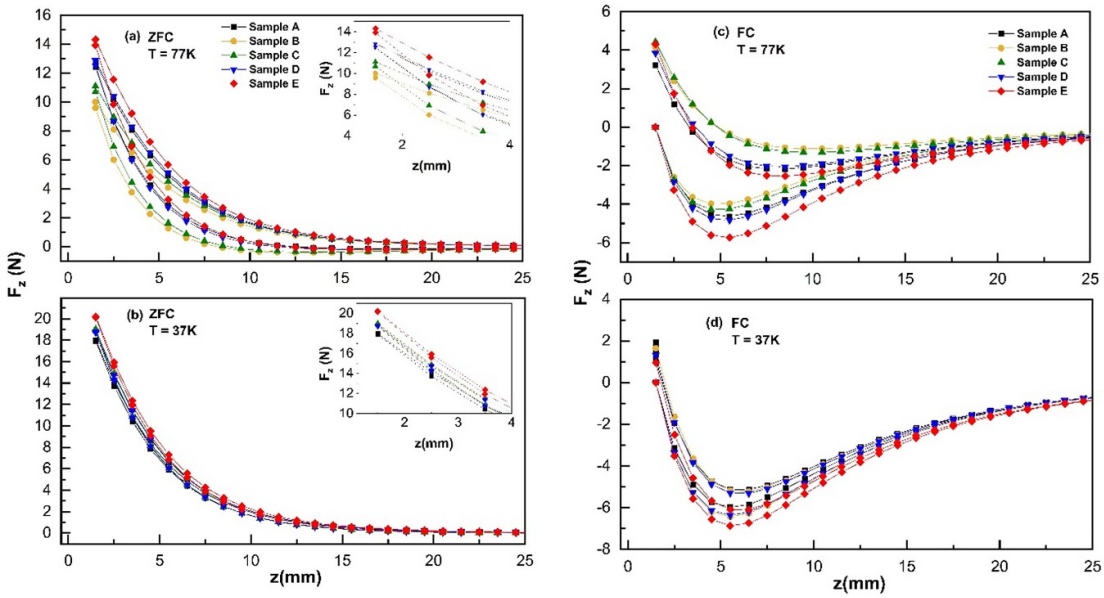

Figure 4. Levitation force F_z (N) versus distance z (mm) in ZFC regime at temperatures (a) 77 K and (b) 37 K and FC regime at temperatures (c) 77 K and (d) 37 K.

sample (A), indicating that the trends observed in the magnetic levitation force measurements are consistent with the critical current density results.

The lateral force F_x, opposing sideways displacement of the superconductor along the x-axis relative to the permanent magnet, must be considered together with the vertical levitation forces. Figure 5 presents the lateral force F_x measured in the FC regime at 77 K and 37 K as a function of the horizontal displacement x (mm). For REBCO superconductors, when the *ab*-plane is oriented parallel to the magnet surface, the measured lateral forces exhibit a distinct hysteresis behavior. Similar to the vertical levitation force results, the hysteresis in the lateral force curves is more pronounced at 77 K, reflecting the lower critical current density and stronger volumetric irreversible flux trapping at this temperature. Among all samples, sample E consistently exhibits the highest lateral force F_z at both 37 K and 77 K. This trend is consistent with the vertical force F_z measurements (see figure 4). This agreement between the lateral and vertical force behavior suggests that the enhanced pinning performance at lower temperature strengthens both the levitation force and the lateral restoring capability of the samples.

3.3. AC susceptibility

The in-phase (χ') and out-of-phase (χ'') components of the AC susceptibility as a function of temperature for the conventional plain sample (A) and laser-machined sample (E) are shown in figures 6(a) and (b), respectively. Samples A and E were selected for susceptibility and subsequent measurements: sample A serves as the plain, non-laser-machined reference, while sample E was chosen due to its superior levitation and lateral force performance among all investigated samples. As is well known, the in-phase component χ' of AC susceptibility represents the dispersion part corresponding to the magnetic shielding property of the superconductor generated by the supercurrents, while the AC losses due to the AC magnetic energy that is converted into heat in the sample, is represented by the out-of-phase component χ''. Ideally, the fundamental susceptibility in superconductors shows a single-step drop in χ' measurements and a single peak in χ'' measurements. However, in granular superconductors, two significant drops and associated two peaks are usually observed in χ' and χ'' measurements as a function of temperature, respectively [55, 56]. In the χ' versus temperature graph, the drop which occurs at a higher temperature corresponds to the intrinsic properties of the grains becoming superconductors during the initial cooling cycle, and associated with shielding of the AC applied magnetic field. The second drop occurs at lower temperature and is referred to as the intergranular coupling, arising from bulk shielding of the sample [55, 57]. This is shown in figure 6(a) where the two-step drop is observed in both samples, A and E. The first drop at higher temperatures is sharper in sample E which may indicate that the distribution of defects and oxygen vacancies is more effective in its intragranular behavior as compared to sample A. This result further confirms that the laser machining did not cause any significant damage in the YBCO

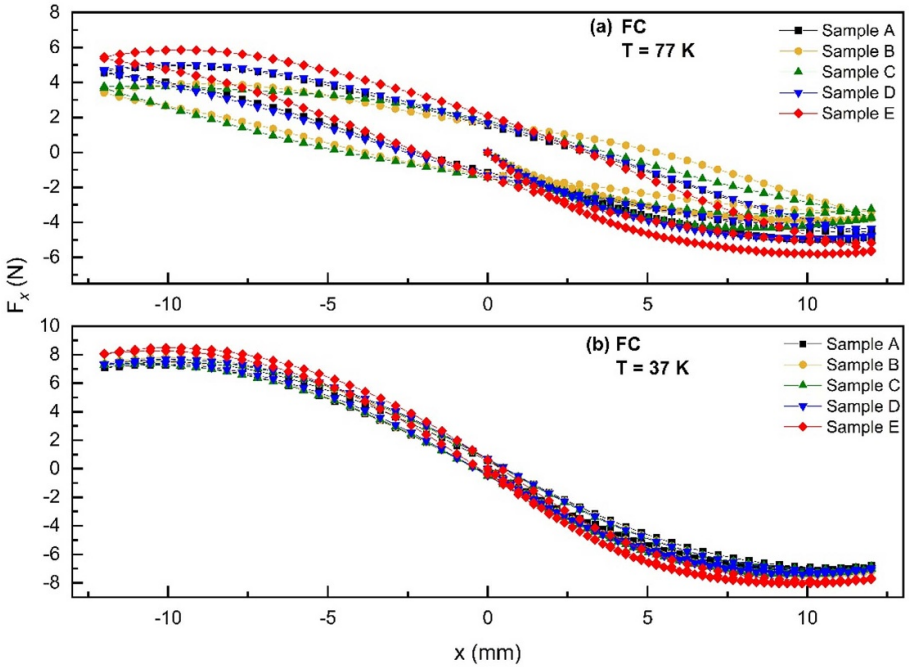

Figure 5. Lateral force F_x (N) versus distance x (mm) in FC regime at temperatures (a) 77 K and (b) 37 K.

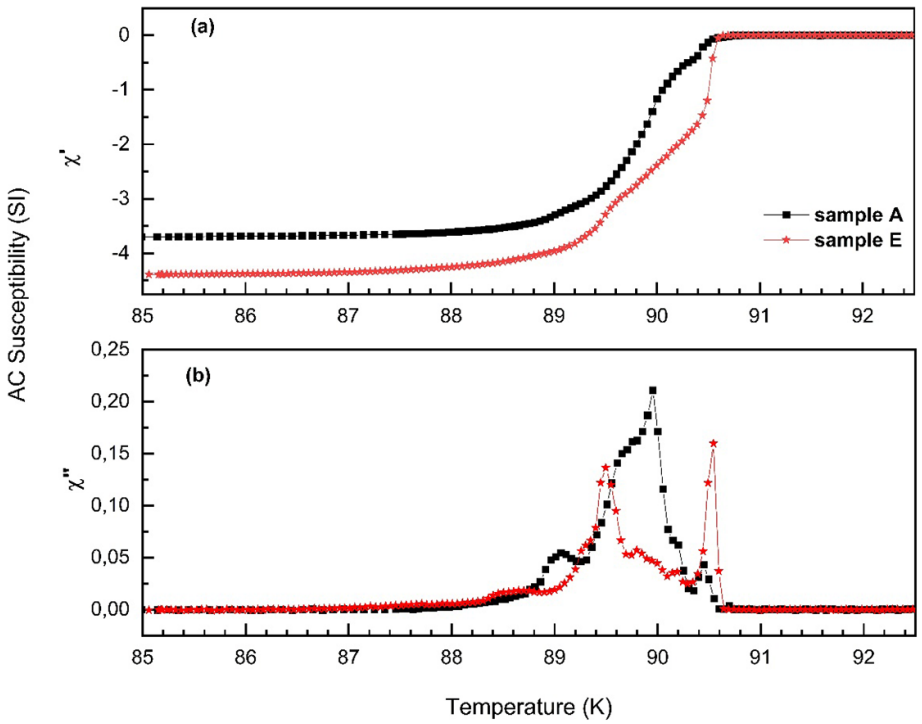

Figure 6. (a) The in-phase (χ') and (b) out-of-phase (χ'') components of the AC susceptibility as a function of temperature of samples A and E, measured with an AC magnetic field amplitude of 0.1 Oe and a frequency of 10 Hz.

grain structure which could otherwise lead to noticeable suppression in the transition critical temperature. Moreover, sample E practically reaches the theoretical diamagnetic limit $\chi' = -4.51$, while sample A is a bit below the corresponding value $\chi' = -4.43$ as calculated from the expression $-1/(1\ \mathrm{N})$ and using the flux metric demagnetizing factors extracted from [58].

The out-of-phase component, χ'', exhibits multiple peaks upon cooling below the superconducting transition temperature, reflecting multiple dissipation mechanisms within the superconducting state. The peak located near the transition temperature is associated with losses arising from the penetration of the

AC magnetic field into the superconducting grains. In general, other peaks exhibited at lower temperatures in the χ'' measurements, known as the inter-grain peak, correspond to the energy loss caused by the penetration of the magnetic field at the intergranular regions. The observed two-step drops in the in-phase component together with the multi-peak behavior in the out-of-phase component confirms the granular nature of the superconducting samples and the distinct roles of intra- and intergranular effects in their observed AC magnetic susceptibility behavior. Figure 6(b), shows that the intra grain peak of sample E is at slightly higher temperature compared to that of sample A which may be attributed to enhanced oxygen content in sample E. The inter-grain peak of sample A, however, appears at a higher temperature than that of sample E and exhibits a greater height with a broader shape, whereas the peak of sample E is sharper and lower in intensity. This suggests that sample E has less energy loss compared to sample A, and this may be attributed to a stronger and more uniform flux pinning and less flux creep, indicating better grain connectivity.

3.4. M–H measurements

Field-dependent DC magnetization (M–H) measurements of samples A and E were carried out in magnetic fields ranging from −7 T to +7 T at temperatures of 37 K, 57 K, and 77 K, as shown in figures 7(a)–(c). All the isothermal magnetic hysteresis loops were measured to study the magnetic interactions in the YBCO structure for both the plain and laser-machined samples. While both samples exhibit typical hysteresis loops, the fishtail effect (or second magnetization peak, SMP) is clearly observed at all measured temperatures in sample E. The appearance of the SMP in sample E may be attributed to a combination of different pinning and structural effects, and it is especially noteworthy that this beneficial feature persists even after machining. The fishtail phenomenon has been reported in several previous studies for different types of superconductors, including $REBa_2Cu_3O_{7-x}$ (RE = Y, Nd, Yb, etc) [59, 60], and it is generally related to several factors rather than a single well-defined mechanism, such as oxygen deficiency, the formation of normal regions acting as pinning centers, a crossover from 3D to 2D pinning mechanisms, the interplay between surface barriers and bulk pinning, enhanced critical current density near crystallite edges, and matching effects associated with defects such as nanocolumns [61].

The critical current densities J_c of samples A and E were calculated using Bean's critical state model assumed for the cylinder geometries [62], with the magnetic field applied perpendicular to the plane of the disc sample, according to the following equation:

$$J_c = \frac{3\Delta M}{2\mathrm{R}}. \tag{1}$$

Here ΔM is the width of the hysteresis loop ($\Delta M = M^+ - M^-$, with M^+ and M^- the measured magnetic moments corresponding to the decreasing and increasing field branches in the magnetic loop, respectively), R is the radius of the disc, and d is its thickness.

The J_c values, calculated using equation (1), versus magnetic field H are shown in figures 7(d)–(f) for samples A and E at 37 K, 57 K, and 77 K. The conventional plain sample A, exhibits the expected behavior of a type-II superconductor, with a monotonic decrease of J_c as the magnetic field increases at both temperatures 37 K and 57 K followed by sharper decrease at higher magnetic fields. The decrease in J_c values is slightly more pronounced at 57 K, reflecting the effect of higher thermal energy on vortex motion. The laser-machined sample E, on the other hand, shows slightly higher J_c values over the full magnetic field range at both temperatures and displays a non-monotonic trend. After an initial drop at low fields, J_c increases to form a broad peak at intermediate fields, characteristic of the SMP that was observed in magnetic hysteresis loops (figures 7(a)–(c)). The SMP at 37 K is shown at about 4.5 T, while at 57 K it is observed at about 3 T, which may be an indication that the field-induced enhancement of vortex pinning becomes relatively stronger as thermal energy begins to influence vortex dynamics. At 77 K, both samples show overall lower J_c values, as expected near the superconducting transition temperature (T_c), due to increased thermal fluctuations weakening vortex pinning. Sample A maintains its monotonic decrease of J_c with field while sample E still exhibits a small enhancement at intermediate fields, but the SMP-related peak is noticeably weaker than at 37 K and 57 K, indicating that the mechanism responsible for the SMP is less effective at higher temperatures. A similar behavior was reported by Zmorayova *et al* [63] who observed the presence of a small SMP in the J_c vs magnetic field curve of a single-grain YBCO sample containing holes in the magnetic field range of 1.5 T to 3.5 T.

Overall, the comparison of the field dependence of the critical current densities for the conventional plain sample A and the laser-machined sample E reveals a clear enhancement of J_c in the laser-machined sample. As shown in the figures 7(d)–(f), sample E consistently exhibits higher J_c values than sample A especially at 37 K and 57 K. This observation indicates that neither the fs laser cutting used to extract

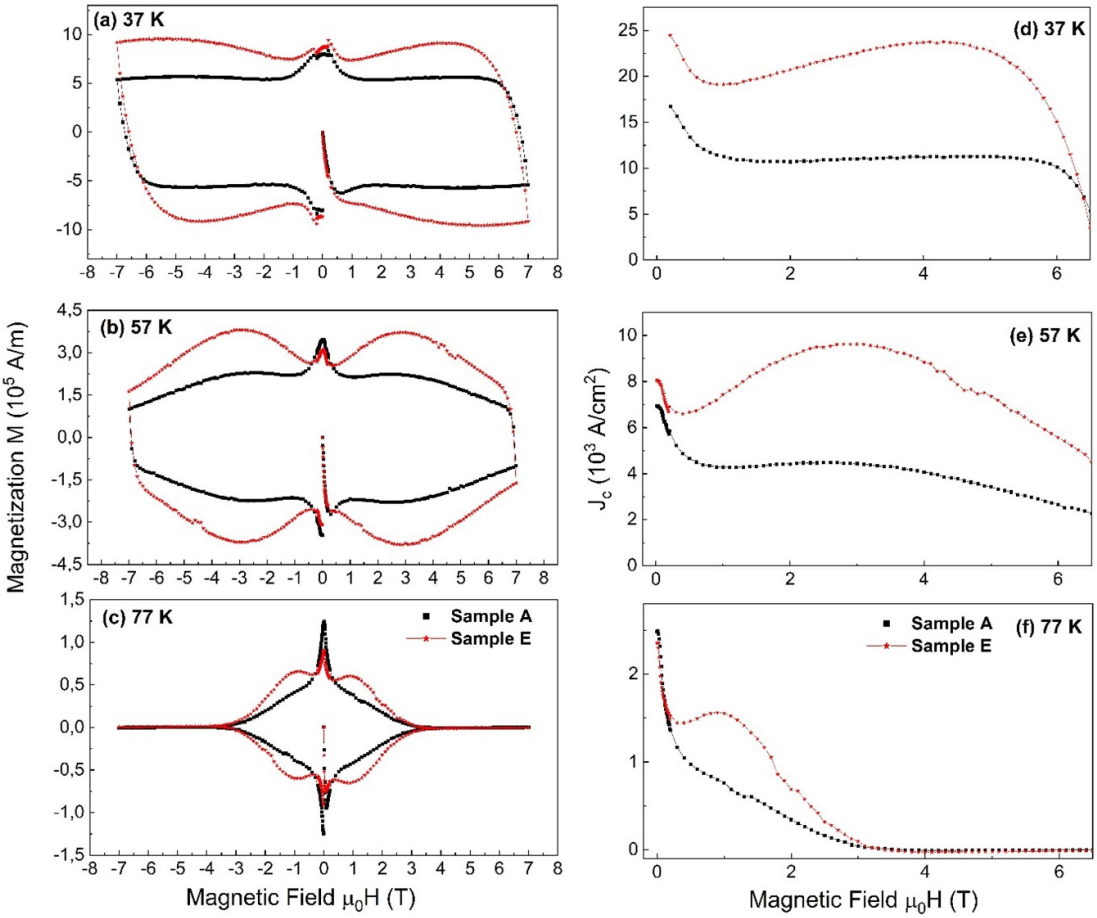

Figure 7. M–H loops and corresponding J_c vs magnetic field for samples A and E at temperatures 37, 57 and 77 K. M–H loops shown in (a)–(c) and J_c data calculated from magnetization hysteresis are shown in (d)–(f).

the measurement discs nor the laser surface machining degrades the superconducting properties. The superconducting performance is not only conserved, but even improved, as shown by the higher J_c values.

4. Conclusion

In this work, YBCO superconductors were successfully fabricated using TSMG method, and 3D laser machining using an ultrashort-pulsed laser was successfully employed to prepare YBCO samples. To the best of our knowledge, this is the first study reporting the application of ultrashort-pulsed laser based on 3D machining to the textured YBCO superconductors to fabricate artificial holes. XRD and SEM analyses show that the laser machining does not induce noticeable changes in the crystal structure or microstructure of the samples, indicating that the laser does not introduce appreciable damage to the interior of samples studied in this study. In addition, the levitation force performance, as well as the magnetic and electrical properties of the laser-machined samples, are similar or even better than those of the pristine fabricated samples. While this enhancement is effectively encouraging, further experimental research facilitates better understanding of physical behavior, where we observed the increased magnetization in M–H hysteresis measurements related with the flux dynamics and increased J_c together with the associated levitation force measurements.

Moreover, these results highlight the potential of ultrashort-pulsed laser machining as a powerful and reliable technique for introducing controlled artificial holes and machine complex geometries into brittle YBCO superconductors without compromising their properties. This capability is attractive for applications, where precise shaping and mechanical stability are essential for optimizing superconducting performance.

Acknowledgment

The authors gratefully acknowledge the financial support provided by Ankara University Scientific Research Projects (BAP) Under Project No FDK-2024-3472. The authors also acknowledge the support of COST Action CA19108. One of the co-authors, PhD student Fatima Almokdad, is grateful to TÜBİTAK for the support Under The Project ID 123N624. The experimental measurements and sample machining were carried out with the support of Recep Tayyip Erdoğan University and Spanish projects PID2020-113034RB-I00 (MCIN/AEI/10.13039/ 501100011033), PID2023-146041OB-C21 (MICIU/AEI/10.13039/501100011033 and ERDF/ EU), and T54-23R (Gobierno de Aragón).

Data availability statement

All data that support the findings of this study are included within the article (and any supplementary files).

Author contributions

F Al-Mokdad 0009-0003-6701-6613
Data curation (equal), Formal analysis (equal), Investigation (equal), Visualization (equal), Writing – original draft (equal), Writing – review & editing (equal)

S B Guner 0000-0001-7487-4817
Conceptualization (equal), Investigation (equal), Methodology (equal), Writing – original draft (equal), Writing – review & editing (equal)

J Rivera-Sahún
Investigation (equal)

A Badía-Majós 0000-0002-8753-2397
Methodology (equal), Writing – review & editing (equal)

L A Angurel 0000-0001-5685-2366
Funding acquisition (equal), Methodology (equal)

G F de la Fuente
Conceptualization (equal), Methodology (equal), Writing – review & editing (equal)

E Martínez 0000-0003-4839-5286
Investigation (equal), Methodology (equal)

L Porta-Velilla
Investigation (equal)

A Gencer
Conceptualization (equal), Funding acquisition (equal), Methodology (equal), Project administration (equal), Supervision (equal), Writing – review & editing (equal)

References

[1] Hull J R and Murakami M 2004 Applications of bulk high-temperature superconductors *Proc. IEEE* **92** 1705–18
[2] Maimaiti N, Abulaiti A and Yang W 2024 The effect of infiltration temperature on the microstructure and magnetic levitation force of single-domain $Yba_2Cu_3O_{7-x}$ bulk superconductors grown by a modified Y+ 011 IG method *Nanomaterials* **15** 21
[3] Namburi D K, Shi Y and Cardwell D A 2021 The processing and properties of bulk (RE) BCO high temperature superconductors: current status and future perspectives *Supercond. Sci. Technol.* **34** 053002
[4] Ali M Z, Zheng J, Huber F, Zhang Z, Yuan W and Zhang M 2020 4.6 T generated by a high-temperature superconducting ring magnet *Supercond. Sci. Technol.* **33** 04LT01
[5] Liu J *et al* 2020 World record 32.35 tesla direct-current magnetic field generated with an all-superconducting magnet *Supercond. Sci. Technol.* **33** 03LT01
[6] Liu X, Ke Z, Cheng Y, Liu Y and Deng Z 2022 Strong magnetic field dependence of micro-YBCO superconductor levitated above Halbach guideway *IEEE Trans. Instrum. Meas.* **71** 1–10
[7] Nouailhetas Q, Xing Y, Dorget R, Dirahoui W, Guijosa S, Trillaud F, Lévêque J, Noudem J G, Labbé J and Berger K 2024 Characterisation of large-sized REBaCuO bulks for application in flux modulation machines *Materials* **17** 3827

[8] Wu M K, Ashburn J R, Torng C J, Hor P H, Meng R L, Gao L, Huang Z J, Wang Y Q and Chu C W 1987 Superconductivity at 93 K in a new mixed-phase Y–Ba–Cu–O compound system at ambient pressure *Phys. Rev. Lett.* **58** 908

[9] Murakami M 2007 Processing and applications of bulk RE-Ba-Cu-O superconductors *Int. J. Appl. Ceram. Technol.* **4** 225–41

[10] Xu A, Jaroszynski J J, Kametani F, Chen Z, Larbalestier D C, Viouchkov Y L, Chen Y, Xie Y and Selvamanickam V 2009 Angular dependence of Jc for YBCO coated conductors at low temperature and very high magnetic fields *Supercond. Sci. Technol.* **23** 014003

[11] Wang J *et al* 2002 The first man-loading high temperature superconducting Maglev test vehicle in the world *Physica C* **378** 809–14

[12] Haugan T J, Puig T, Matsumoto K and Wu J 2020 Artificial pinning centers in (Y, RE)-Ba-Cu-O superconductors: recent progress and future perspective *Supercond. Sci. Technol.* **33** 040301

[13] Mele P, Matsumoto K, Horide T, Ichinose A, Mukaida M, Yoshida Y, Horii S and Kita R 2008 Ultra-high flux pinning properties of BaMO3-doped $YBa_2Cu_3O_{7-x}$ thin films (M = Zr, Sn) *Supercond. Sci. Technol.* **21** 032002

[14] Matsumoto K and Mele P 2010 Artificial pinning center technology to enhance vortex pinning in YBCO coated conductors *Supercond. Sci. Technol.* **23** 014001

[15] Haugan T, Barnes P N, Maartense I, Cobb C B, Lee E J and Sumption M 2003 Island growth of Y_2BaCuO_5 nanoparticles in (211 $\sim$ 1.5 nm/123 $\sim$ 10 nm) $\times$ N composite multilayer structures to enhance flux pinning of $YBa_2Cu_3O_{7-\delta}$ films *J. Mater. Res.* **18** 2618–23

[16] Li G Z, Wang M and Yang W M 2015 Enhanced superconducting properties in infiltration processed Y-Ba-Cu-O single-grain superconductor with nano-sized pinning centers *J. Alloys Compd.* **649** 559–63

[17] Sueyoshi T, Enokihata R, Yamaguchi H, Fujiyoshi T, Okuno Y and Ishikawa N 2021 Summation of flux pinning by columnar defects tilted at different angles in YBCO thin films *IEEE Trans. Appl. Supercond.* **31** 1–5

[18] Kirchner A, Espenhahn T, Klug S, Nielsch K and Hühne R 2024 Comparison of levitation properties between bulk high-temperature superconductor blocks and high-temperature superconductor tape stacks prepared from commercial coated conductors *Materials* **17** 4516

[19] Abdioglu M, Ozturk K, Gedikli H A, Ekici M E and Cansiz A 2015 Levitation and guidance force efficiencies of bulk YBCO for different permanent magnetic guideways *J. Alloys Compd.* **630** 260–5

[20] Yang W M, Chao X X, Bian X B, Liu P, Feng Y, Zhang P X and Zhou L 2003 The effect of magnet size on the levitation force and attractive force of single-domain YBCO bulk superconductors *Supercond. Sci. Technol.* **16** 789

[21] Yang W M *et al* 1998 The effect of excess Y_2O_3 addition on the levitation force of melt processed YBCO bulk superconductors *Physica* C **305** 269–74

[22] Yang W M, Zhou L, Feng Y, Zhang P X, Zhang C P, Nicolsky R and de Andrade J R 2002 The effect of different field cooling processes on the levitation force and attractive force of single-domain $YBa_2Cu_3O_7$−x bulk *Supercond. Sci. Technol.* **15** 1410

[23] Noudem J G, Meslin S, Harnois C, Chateigner D and Chaud X 2004 Melt textured $YBa_2Cu_3O_\gamma$ bulks with artificially patterned holes: a new way of processing *c*-axis fault current limiter meanders *Supercond. Sci. Technol.* **17** 931

[24] Dias D H N, Sotelo G G, Moysés L A, Telles L G T, Bernstein P, Kenfaui D, Aburas M, Chaud X and Noudem J G 2015 Application of textured YBCO bulks with artificial holes for superconducting magnetic bearing *Supercond. Sci. Technol.* **28** 075005

[25] Lousberg G P, Fagnard J F, Ausloos M, Vanderbemden P and Vanderheyden B 2010 Modification of the trapped field in bulk high-temperature superconductors as a result of the drilling of a pattern of artificial columnar holes *J. Phys.: Conf Ser.* **234** 012023

[26] Noudem J G, Meslin S, Horvath D, Harnois C, Chateigner D, Eve S, Gomina M, Chaud X and Murakami M 2007 Fabrication of textured YBCO bulks with artificial holes *Physica* C **463** 301–7

[27] Diko P, Kračunovská S, Ceniga L, Bierlich J, Zeisberger M and Gawalek W 2005 Microstructure of top seeded melt-grown YBCO bulks with holes *Supercond. Sci. Technol.* **18** 1400

[28] Radušovská M, Diko P, Hajdová P, Volochová D, Antal V, Hlásek T, Plecháček V and Antončík F 2022 Bulk GdBCO-Ag superconductors with holes *J. Am. Ceram. Soc.* **105** 7822–30

[29] Martirosian I, Pokrovskii S, Egorov A and Mavritskii O 2024 Non-stationary structural changes in HTS composites under the influence of high-intensity femtosecond laser pulses *Supercond. Fundam. Appl. Res.* **58** 58–77

[30] Hajdova P, Diko P, Rajňák M, Bednarčík J, Antal V, Kucharova V, Zmorayova K and Radušovská M 2021 The influence of CeO_2 addition on microstructure and superconducting properties of GdBCO-Ag single grain bulk superconductors *J. Alloys Compd.* **889** 161697

[31] Naik S P K *et al* 2022 Investigation of high-energy ultrasonication of RE_2BaCuO_5 (RE = Y, Gd) on the growth and superconducting properties of REBa2Cu3O7-δ top-seeded *Supercond. Sci. Technol.* **35** 074003

[32] Kim C J, Kim K-B, Hong G-W, Won D-Y, Kim B-H, Kim C-T, Moon H-C and Suhr D-S 1992 Microstructure, microhardness, and superconductivity of CeO_2-added Y-Ba-Cu-O superconductors *J. Mater. Res.* **7** 2349–54

[33] Guner S B, Celik S and Tomakin M 2017 The investigation of magnetic levitation performances of single grain YBCO at different temperatures *J. Alloys Compd.* **705** 247–52

[34] Savaskan B, Guner S B, Yamamoto A and Ozturk K 2020 Trapped magnetic field and levitation force properties of multi-seeded YBCO superconductors with different seed distance *J. Alloys Compd.* **829** 154400

[35] Shi Y, Mousavi T, Dennis A R, Ainslie M D, Speller S C, Grovenor C R and Durrell J H 2022 The effect of facet lines on critical current density and trapped field in bulk RE–Ba–Cu–O single grains *Supercond. Sci. Technol.* **35** 105002

[36] Leblond C, Monot I, Provost J and Desgardin G 1999 Optimization of the texture formation and characterization of large size top-seeded-melt-grown YBCO pellets *Physica C* **311** 211–22

[37] Baumann J, Shi Y, Weerakonda D, Durrell J H and Cardwell D A 2023 Understanding the porosity and its effects on the superconducting properties of YBCO single grains *J. Eur. Ceram. Soc.* **43** 1542–7

[38] Shi Y, Hari Babu N and Cardwell D A 2005 Development of a generic seed crystal for the fabrication of large grain (RE)–Ba–Cu–O bulk superconductors *Supercond. Sci. Technol.* **18** L13–L16

[39] Auguste F, Vandewalle N, Ausloos M, Macmanus-Driscoll J, Rulmont A and Cloots R 1998 The Nd-123 superconducting system: from single crystal to top-seeded large grain. Physical and chemical parameters influence *Appl. Supercond.* **6** 77–85

[40] Kim C J, Kim K B, Kuk I H, Hong G W, Lee Y S and Park H S 1997 Microstructure change during oxygen annealing and the effect on the levitation force of melt-textured Y-Ba-Cu-O superconductors *Supercond. Sci. Technol.* **10** 947–54

[41] Zheng M H, Xiao L, Ren H T, Jiao Y L and Chen Y X 2003 Study of oxygenation process during the preparation of single domain YBCO bulk superconductors *Physica C* **386** 258–61

[42] Abdioglu M, Guner S B, Ozturk K, Yang C, Chen I and Celik S 2022 Magnetic levitation force and trapped field properties of multiseeded YBCO with triangular arrangement of seeds *Int. J. Appl. Ceram. Technol.* **19** 459–66

[43] Yang W M and Wang M 2013 New method for introducing nanometer flux pinning centers into single domain YBCO bulk superconductors *Physica C* **493** 128–31
[44] Daeumling M, Seuntjens J M and Larbalestier D C 1990 Oxygen-defect flux pinning, anomalous magnetization and intra-grain granularity in $YBa_2Cu_3O_{7-\delta}$ *Nature* **346** 332–5
[45] Matsushita T 2000 Flux pinning in superconducting 123 materials *Supercond. Sci. Technol.* **13** 730–7
[46] Celik S 2016 Design of magnetic levitation force measurement system at any low temperatures from 20 K to room temperature *J. Alloys Compd.* **662** 546–56
[47] International Centre for Diffraction Data (ICDD) Powder Diffraction File PDF no. 01–078-2129
[48] Wei G, Guisheng Z, Xiao C, Aiping W, Minghui Z, Yulei J and Jialie R 2012 The study of multiple thermal cycle of HTS YBCO bulk *Physica C* **474** 25–28
[49] International Centre for Diffraction Data (ICDD) Powder Diffraction File PDF no. 01–078-2214
[50] Benzi P, Bottizzo E and Rizzi N 2004 Oxygen determination from cell dimensions in YBCO superconductors *J. Cryst. Growth* **269** 625–9
[51] Barood F *et al* 2023 Orthorhombic $YBa_2Cu_3O_7-\delta$ superconductor with TiO_2 nanoparticle addition: crystal structure, electric resistivity, and AC susceptibility *Coatings* **13** 1093
[52] Sahoo B, Mohapatra S R, Singh A K, Samal D and Behera D 2019 Effects of CNTs blending on the superconducting parameters of YBCO superconductor *Ceram. Int.* **45** 7709–16
[53] Azzouz F B, Zouaoui M, Mani K D, Annabi M, Van Tendeloo G and Salem M B 2006 Structure, microstructure and transport properties of B-doped YBCO system *Physica C* **442** 13–19
[54] Bean C P 1964 Magnetization of high-field superconductors *Rev. Mod. Phys.* **36** 31
[55] Goldfarb R B, Clark A F, Braginski A I and Panson A J 1987 Evidence for two superconducting components in oxygen-annealed single-phase Y Ba Cu O *Cryogenics* **27** 475–80
[56] Ghazanfari N, Kılıç A, Gencer A and Özkan H 2007 Effects of Nb_2O_5 addition on superconducting properties of BSCCO *Solid State Commun.* **144** 210–4
[57] Çelebi S E, Karaca I, Aksu E and Gencer A 1998 Frequency dependence of the intergranular AC loss peak in a high-Tc Bi–(Pb)–Sr–Ca–Cu–O bulk superconductor *Physica C* **309** 131–7
[58] Chen D X, Brug J A and Goldfarb R B 1991 Demagnetizing factors for cylinders *IEEE Trans. Magn.* **27** 3601–19
[59] Werner M, Sauerzopf F M, Weber H W and Wisniewski A 2000 Fishtail effect in the magnetization of superconducting $RBa_2Cu_3O_{7-\delta}$ (R = Y, Nd, Yb) and $Y_2Ba_4Cu_8O_{16}$ single crystals *Phys. Rev. B* **61** 14795
[60] Shit S, Namburi D K, Das S D and Nath T K 2024 Revealing the vortex phases and second magnetization peaks in SmBCO superconductors *J. Appl. Phys.* **136** 17
[61] Ruiz H S *et al* 2026 Critical current density in advanced superconductors *Prog. Mater. Sci.* **155** 101492
[62] Sanchez A and Navau C 2001 Critical-current density from magnetization loops of finite high-Tc superconductors *Supercond. Sci. Technol.* **14** 444
[63] Zmorayova K, Diko P, Volochová D, Antal V, Hlásek T, Plecháček V and Antončík F 2023 Complex microstructural analysis of YBCO single-grain bulks with artificial holes: effect on superconducting properties *Ceram. Int.* **49** 22177–86